

# Surface-Plasmon Enhanced Near-Bandgap Light Absorption in Silicon Photovoltaics

Lu Hu, Xiaoyuan Chen, and Gang Chen\*

*Massachusetts Institute of Technology, Cambridge, MA 02139, USA*

An extended Mie scattering theory is used in this paper to analyze the surface-plasmon enhanced light absorption in silicon for photovoltaic applications. The calculation results show that the optical absorption in silicon can be enhanced up to 50 times at resonance frequency by embedded spherical silver nanoparticles due to the local field enhancement by surface plasmons. The analysis reveals that the surface-plasmon field is concentrated in a spherical shell that encloses the particle. The enhancement reaches maximum when the thickness of the shell is 0.26 times the radius of the particle. The maximum absorption enhancement is found to be induced by silver particles with intermediate radii. The enhancement with larger particles is limited by the retardation effect, while the smaller-particle assisted absorption is hampered by electron scattering on the particle surface.

**Keywords:** Surface Plasmon, Solar Photovoltaics, Silver Nanoparticle, Mie Scattering.

## 1. INTRODUCTION

One key challenge for silicon-based solar cells is the weak absorption of long-wavelength photons near the bandgap (1.1 eV) due to the indirect bandgap of silicon.<sup>1,2</sup> A large fraction of the AM 1.5 solar spectrum falls into a regime (0.7 μm–1.1 μm) where silicon does not absorb light well.<sup>3</sup> The capture of these long-wavelength photons imposes a particular problem to the thin-film silicon solar cells. For this reason, thin-film silicon solar cells often incorporate some forms of light trapping mechanisms.

As the optical absorption rate in a lossy medium depends on the optical path length and the local electric field intensity, two different light trapping strategies have been developed. The most widely used strategy for light trapping is applying complex textures on the back or the front surfaces of the cells.<sup>4</sup> The surface textures diffuse the incoming light and enhance the absorption by increasing the optical path length of the photons. It was not until recently that another light trapping strategy—increasing the local field intensity via surface-plasmons using metal nanoparticles—started to receive attentions.<sup>5–8</sup> Plasmons are collective oscillations of the conduction band electrons excited by incident electromagnetic waves.<sup>9</sup> Surface plasmons are bounded to the interface when the dielectric constants of the two sides satisfy certain conditions, depending on the geometry.<sup>10</sup> These localized surface

modes are supported in noble metals such as gold and silver. It has long been observed that surface plasmons can lead to significant electric field enhancement near the surface and thus increase the rate of any processes that depend on the field intensity. One well-known example is the surface-plasmon enhanced Raman scattering, where the Raman signals, proportional to the fourth-power of the electric field, can be increased many orders of magnitude using metallic nanoparticles such as silver.<sup>11</sup> Similar mechanisms can be applied to photovoltaic cells for light trapping. Instead of using surface textures, noble metal particles are either placed on the surface as in the case of silicocn<sup>5,6</sup> or embedded in the active regions as in the case of polymer-based solar cells<sup>7</sup> and dye-sensitized solar cells<sup>8</sup> as localized photon absorption centers. Experimental results show considerable increase of photo currents, especially in the long wavelength regime.<sup>5–7</sup>

Despite the reported enhancement, to our best knowledge, detailed analyses of the surface-plasmon enhanced optical absorption are lacking for photovoltaic applications. Past research efforts rely on either simple dipole models, or numerical simulations. Catchpole et al. used a dipole scattering model which does not apply to large particles.<sup>12</sup> Derkacs et al. performed finite-element electromagnetic simulations for a single gold particle at a fixed wavelength.<sup>5</sup> Rand et al. analyzed the field enhancement using two-dimensional finite-element simulations.<sup>7</sup> In this paper, we take an analytical approach and study the absorption enhancement by silver nanoparticles embedded

\*Author to whom correspondence should be addressed.

in silicon, using an extended Mie scattering theory for a sphere embedded in absorbing media.<sup>13,14</sup> The extended Mie scattering theory takes into account the near field components without making any far field approximations,<sup>15</sup> which ensures the localized surface modes can be represented in the model. A single particle analysis is performed as it reveals fundamental mechanisms of the absorption enhancement, although in real applications, multiple metal nanoparticles are deployed instead of a single particle. In photovoltaic applications the metal articles are usually randomly distributed and the primary enhancement mechanism is the localized surface modes which are less affected by the incoherent scattered light from the randomly spaced neighbors. Therefore, the results obtained from the parametric study of a single particle can serve as the first-order input parameters for the design of more complex structures involving multiple particles. In our calculations, we choose silver nanoparticles as the photon absorption centers because the plasma frequency of silver is the lowest among noble metals,<sup>16</sup> which is ideal for solar photovoltaic applications. Our calculation shows that with the presence of a silver nanoparticle, the net absorption enhancement in silicon can be up to 50 times in the long wavelength regime. The dependence of absorption enhancement on the particle sizes shows a non-monotonic trend. Maximum enhancement is found for particles with intermediate sizes. Larger particles lead to lower enhancement, due to the retardation effect of the electromagnetic waves. Particles with radii smaller than the optimized radius give smaller enhancement, which is due to the size effects caused by boundary scattering of electrons. In addition to the extended Mie theory, we present simplified models for absorption analysis based on dipole models, which is found to be good approximations for particles with small radii. Our analysis also suggests that the absorption by the silver nanoparticle itself is significant, which should be addressed in the future.

## 2. EXTENDED MIE SCATTERING THEORY

Figure 1 shows a schematic illustration of the present analysis. The gray sphere represents a silver particle with a radius of  $a$ . Region 1 is inside the silver sphere and region 2 is in the host absorbing medium, i.e., silicon. The angle  $\theta$  is the zenith angle and  $\Phi$  is the azimuth angle. An imaginary sphere with a radius of  $R$  is also drawn as we will analyze the absorption in silicon within this radius. A plane wave is propagating in the positive  $z$  direction. Without the loss of generality, we choose the electric field of the plane wave to be polarized in the  $x$  direction. The electric and magnetic fields of the incident plane wave are given by

$$\vec{E}_i = E_0 e^{jk_2 r \cos \theta} \hat{e}_x \quad (1)$$

$$\vec{H}_i = \frac{k_2}{\omega \mu_2} E_0 e^{jk_2 r \cos \theta} \hat{e}_y \quad (2)$$

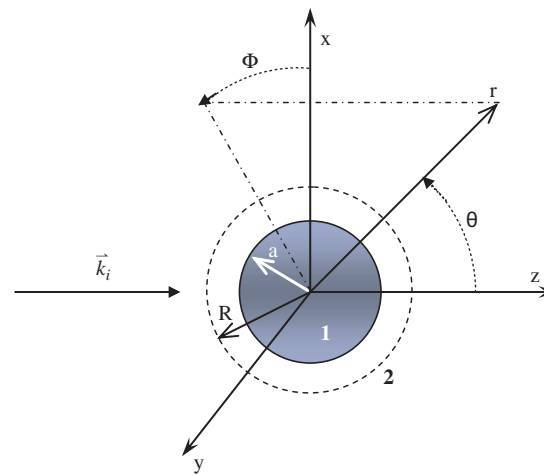


**Fig. 1.** Schematic drawing of a silver particle (region 1) embedded in silicon (region 2). The gray sphere is the silver particle, which is enclosed by an imaginary spherical shell.

where  $E_0$  is the amplitude of the electric field at  $z = 0$ ,  $k_2$  the wave vector of the incident plane wave,  $r$  the radial coordinate,  $\omega$  the angular frequency,  $\mu_2$  the permeability,  $j$  the imaginary unit,  $\hat{e}_x$  the unit vector in the  $x$  direction, and  $\hat{e}_y$  the unit vector in the  $y$  direction. The wave vector is given by  $k_2 = 2N_2\pi/\lambda$ , where  $N_2$  is the optical constant of silicon and  $\lambda$  is the wavelength in vacuum. Since neither silver nor silicon is magnetic material, we have  $\mu_1 = \mu_2 = \mu_0$ , where subscripts 1, 2 and 0 denote regions 1, 2 and vacuum. Following procedures in Ref. [13], the scattered field can be expanded into vector spherical harmonics

$$\vec{E}_s = \sum_{n=1}^{\infty} E_n (j a_n \vec{N}_{e1n}^{(3)} - b_n \vec{M}_{o1n}^{(3)}) \quad (3)$$

$$\vec{H}_s = \frac{k_2}{\omega \mu_0} \sum_{n=1}^{\infty} E_n (j b_n \vec{N}_{o1n}^{(3)} + a_n \vec{M}_{e1n}^{(3)}) \quad (4)$$

where  $\vec{M}$  and  $\vec{N}$  are vector spherical harmonics,  $E_n = j^n E_0 (2n+1)/n(n+1)$ ,  $a_n$  and  $b_n$  are the expansion coefficients, and the subscripts  $e$  and  $o$  denote even and odd. The definitions of the vector spherical harmonics and the derivations of the expansion coefficients are not given here since Ref. [13] contains detailed information. Note that the scattered field and the expansion coefficients derived in Ref. [13] can be directly applied to the absorbing host media by treating the optical constant of the host media as complex number. We can now define the field enhancement by

$$\eta(\vec{r}) = \frac{|\vec{E}_2(\vec{r})|}{|\vec{E}_i(\vec{r})|} = \frac{|\vec{E}_i(\vec{r}) + \vec{E}_s(\vec{r})|}{|\vec{E}_i(\vec{r})|} \quad (5)$$

where  $r > a$ .

The rate of energy absorption in a sphere with radius  $R$  is obtained by integrating the Poynting vector over the surface of the sphere<sup>14</sup>

$$W_{\text{abs}}(R) = \frac{\pi |E_0|^2}{\mu_0 \omega |k_2|^2} \operatorname{Re} \left\{ k_2^* \sum_{n=1}^{\infty} (2n+1) \right. \\ \times [j\psi_n^* \psi'_n - j\psi_n \psi'^*_n + jb_n \psi_n^* \xi_n + jb_n^* \psi_n \xi'_n \\ + j|a_n|^2 \xi'_n \xi_n - j|b_n|^2 \xi_n \xi'^*_n \\ \left. - ja_n \psi_n^* \xi'_n - ja_n^* \psi_n^* \xi_n^*] \right\} \quad (6)$$

where  $\psi_n$  and  $\xi_n$  are the Riccati-Bessel functions, and  $\psi'_n$  and  $\xi'_n$  are their derivatives. The symbol  $\operatorname{Re}$  means the real component. The superscript \* denotes the complex conjugate. Note that the absorption rate given in Eq. (6) differs from the standard Mie scattering theory<sup>13</sup> in terms of additional cross terms, due to the fact that the host medium is absorbing. For non-absorbing host media, the cross terms vanish and Eq. (6) goes back to the standard form. By energy balance, the absorption rate in the silicon spherical shell ( $a < r < R$ ) is then given by

$$\Delta W_{\text{abs}} = W_{\text{abs}}(R) - W_{\text{abs}}(a) \quad (7)$$

Note that the absorption by the silver sphere is excluded because the photon energy absorbed in the sphere converts to heat and does not generate electricity.

To obtain the absorption enhancement, the absorption inside homogeneous silicon host medium (without the presence of a silver particle) needs to be calculated. In homogeneous medium, the scattering field is zero and the total field is identical to the incident field. The absorption inside of a spherical region with radius  $r$  is obtained by integrating the Poynting vector over the sphere surface

$$W_{\text{abs}, \text{Si}} = \int_0^{2\pi} \int_0^\pi \frac{1}{2} \operatorname{Re}(\vec{E}_i \times \vec{H}_i^*) \cdot (-\hat{r}) r^2 \sin\theta \cos\theta d\theta d\Phi \\ = \frac{\pi \operatorname{Re}(k_2) |E_0|^2 r^2}{\mu_0 \omega} \left[ \frac{\cosh(2k_2'' r)}{k_2'' r} - \frac{\sinh(2k_2'' r)}{2(k_2'' r)^2} \right] \quad (8)$$

where  $k_2''$  is the imaginary part of the incident wave vector. The absorption enhancement factor is defined as the ratio of Eqs. (7) and (8)

$$\gamma(R, a) = \frac{\Delta W_{\text{abs}}(R, a)}{W_{\text{abs}, \text{Si}}(R)} \quad (9)$$

The optical constants are important input parameters for computing the electromagnetic fields. For the calculation of the enhancement factor, we take the experimentally measured optical constants of silicon from Ref. [17]. At room temperature, the mean free path of electrons in bulk silver is around 40 nm.<sup>9</sup> Since in this work the diameter of the silver particles of interest is on the same order or smaller than the mean free path of the electrons, the collision of the electrons with the particle surface

becomes important as an additional relaxation process.<sup>18</sup> The dielectric function of small silver particles should thus be modified to take account for the free electron boundary scattering, which is expressed as<sup>19</sup>

$$\varepsilon(\omega) = \varepsilon_{\text{bulk}}(\omega) + \frac{\omega_p^2}{\omega^2 + j\Gamma_{\text{bulk}}\omega} - \frac{\omega_p^2}{\omega^2 + j\Gamma\omega} \quad (10)$$

where  $\Gamma_{\text{bulk}}$  is the damping constant of bulk silver,  $\Gamma$  is the modified damping constant,  $\varepsilon_{\text{bulk}}$  is bulk dielectric function of silver from Ref. [17], and  $\omega_p$  is the plasma frequency. For silver,  $\omega_p = 14.0 \times 10^{15}$  rad/s.<sup>16</sup> The last two terms in Eq. (10) represent the modification to the free electron part in the dielectric function. The second term cancels the free electron contribution in the bulk medium, while the last term includes electron collisions in bulk materials as well as with the surface, by modifying the damping constant,

$$\Gamma = \Gamma_{\text{bulk}} + A v_F / a \quad (11)$$

where  $A = 1$  and  $1/\Gamma_{\text{bulk}} = 31 \times 10^{-15}$  s,<sup>16,19</sup> and  $v_F = 1.39 \times 10^6$  m/s is the Fermi velocity of electrons in silver.<sup>9</sup> Equation (10) ensures that experimental data on the dielectric constant, which includes other optical transitions, can be used directly.

### 3. CALCULATION RESULTS AND DISCUSSION

The electric field of surface plasmons is known to concentrate only near the surface and decays rapidly when moving away from the surface, which naturally raises the question regarding the net absorption enhancement. To quantify the effects of field concentration on the absorption, the enhancement factors as defined in Eq. (9) are plotted in Figure 2 in log scale for silver particles with different radii. The wavelength of the incident plane wave is

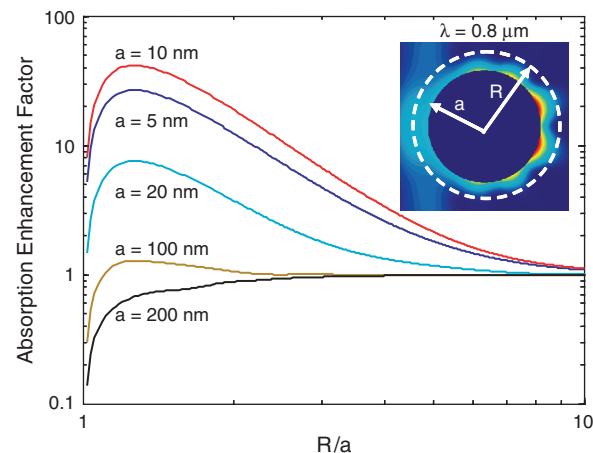


**Fig. 2.** The absorption enhancement factors of silver particles with different sizes. The wavelength of the incident wave is  $0.8 \mu\text{m}$ . The radius of the particle is  $a$  and the outer shell has a radius of  $R$  as shown in the insert. Note  $R$  is normalized to  $a$ .

set at  $0.8 \mu\text{m}$ , which is the plasmon resonance wavelength of small silver particles embedded in silicon, as we will show later. Note the radius  $R$  of the outer shell is normalized to the radius of the sphere. At  $R = a$ , the enhancement factors for all particles are zero (not shown in the figure due to the log scale) because the imaginary silicon spherical shell has zero thickness. When  $R$  increases to a large value, the near field effect diminishes and the enhancement factors for all cases approach 1. In the intermediate range of  $R$ , the enhancement factors reach maximum for all particles except the 200 nm one, which increases monotonically with  $R$  and never exceeds 1. As shown in the figure, smaller particles lead to larger enhancement. However, the dependence of the enhancement factor on the particle radius does not follow a monotonic trend. The 10 nm particle gives the maximum enhancement while the larger 20 nm and smaller 5 nm particles yield less enhancement. The peaks for the 5 nm and 10 nm particles are both at  $R = 1.26a$ , which suggests that the field enhancement is concentrated in a spherical shell with a thickness of  $0.26a$ .

At the wavelength of  $0.8 \mu\text{m}$ , the distribution of the normalized field, or field enhancement (given by Eq. (5)), outside the 100 nm, 10 nm and 5 nm (radius) particles at the  $y = 0$  plane is shown in Figures 3(a–c). Note  $0.8 \mu\text{m}$  is the wavelength in vacuum and it is around  $0.22 \mu\text{m}$  in silicon. The field pattern around the 100 nm particle clearly shows the retardation effects of the electric field, which is anticipated because the wavelength is smaller than the particle diameter such that the interference of the scattered light is strong. As shown in the figure, the field enhancement for the 100 nm particle is rather limited and scatters around the particle surface, which is mainly due to the interference effects. Compared to the 100 nm particle, the fields around the 10 nm and 5 nm particles show a typical pattern of a dipole field and have much higher enhancement factor. The electric field is concentrated around the top and bottom of the particles where the vector of the electric field of the incident wave has the maximum component along the surface normal.

An interesting observation from Figures 3(b and c) is that the fields around the small particles (with radii of 5 nm and 10 nm) share similar distribution patterns that differ only in magnitude. Since for the 5 nm and 10 nm particles, the wavelength is more than 10 times larger than the particle diameters, the dipole model is considered to be a reasonable approximation. The field of an oscillating dipole is given by<sup>20</sup>

$$\vec{E} = \frac{e^{ik_2 r}}{4\pi\epsilon_0\epsilon_2} \left\{ \frac{k_2^2(\hat{e}_r \times \vec{p}) \times \hat{e}_r}{r} + [3\hat{e}_r(\hat{e}_r \cdot \vec{p}) - \vec{p}] \times \left( \frac{1}{r^3} - \frac{jk_2}{r^2} \right) \right\} \quad (12)$$

where  $\epsilon_0$  is the permittivity of vacuum,  $\epsilon_2$  is the relative permittivity of silicon, and  $\hat{e}_r$  is unit vector in

the  $r$  direction. The dipole moment of the particle is expressed as

$$\vec{p} = p\hat{e}_x = 4\pi\epsilon_0\epsilon_2 E_0 a^3 \frac{\epsilon_1 - \epsilon_2}{\epsilon_1 + 2\epsilon_2} \hat{e}_x \quad (13)$$

where  $\epsilon_1$  is the relative permittivity of the silver particle. Since  $\lambda \gg a$ , the field near the particle surface is dominated by the near field terms and Eq. (12) can be

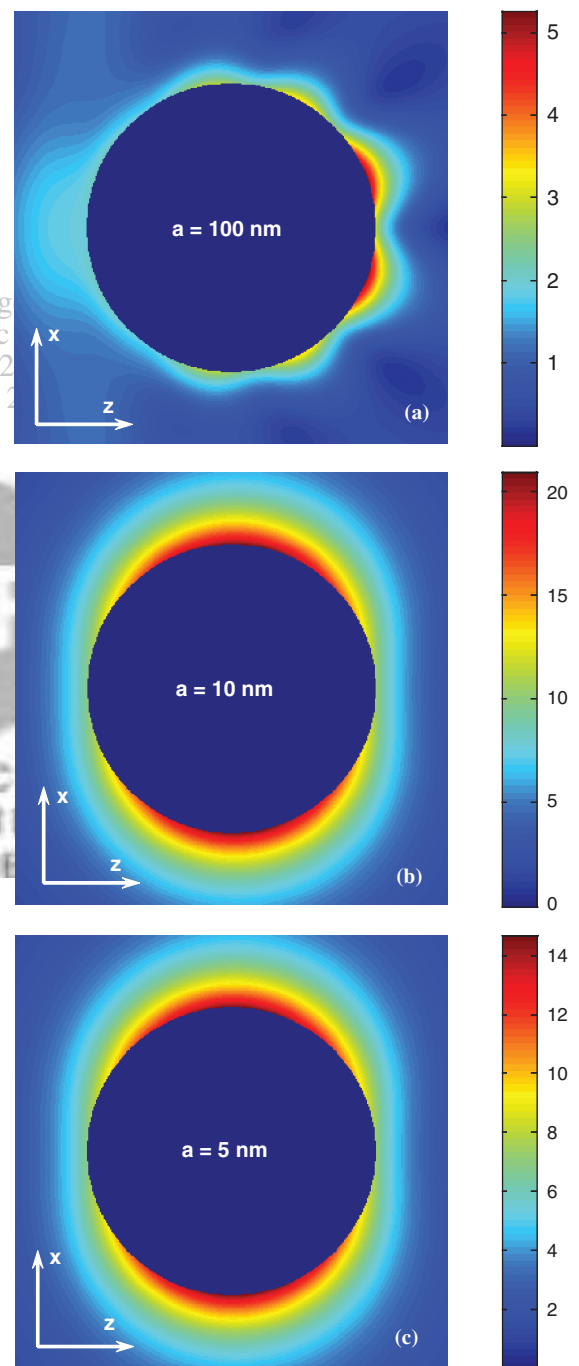


**Fig. 3.** The field distributions outside the silver particles at the  $y = 0$  plane. The field distributions are normalized to the incident plane wave as defined in Eq. (5). (a) 100 nm particle (b) 10 nm particle (c) 5 nm particle.

simplified as

$$\vec{E} = \frac{1}{4\pi\epsilon_2\epsilon_0 r^3} [3\hat{e}_r(\hat{e}_r \cdot \vec{p}) - \vec{p}] \quad (14)$$

Substituting Eq. (13) into Eq. (14) leads to

$$|E| = \left| E_0 \frac{\epsilon_1 - \epsilon_2}{(\epsilon_1 + 2\epsilon_2)} \right| \sqrt{3 \sin^2 \theta \cos^2 \Phi + 1} \left( \frac{a}{r} \right)^3 \quad (15)$$

It is obvious that the distribution profile of the electric field only depends on  $\sqrt{(4 \sin^2 \theta + \cos^2 \theta) \cos^2 \Phi + \sin^2 \Phi (a/r)^3}$ , which explains the similarity between Figures 3(b) and (c). The magnitude of the electric field is given by  $|E_0(\epsilon_1 - \epsilon_2)/(\epsilon_1 + 2\epsilon_2)|$ , which depends on the radius of the particle, since  $\epsilon_2$  is a function of  $a$  due to the electron scattering at the particle surface. Figure 4 shows  $|(\epsilon_1 - \epsilon_2)/(\epsilon_1 + 2\epsilon_2)|$  for selective particles with small radii where the dipole approximation is expected to hold with acceptable accuracy. All the curves show peaks around  $0.8 \mu\text{m}$ , which is the resonance plasmon wavelength when the denominator  $(\epsilon_1 + 2\epsilon_2)$  approaches zero.

Furthermore, using the dipole approximation, the absorption in the silicon shell (Eq. (7)) has a closed analytical form

$$\Delta W_{\text{abs}}(R, a) = \int_0^{2\pi} \int_0^\pi \int_a^R \frac{1}{2} \epsilon_2'' |E|^2 |r^2 \sin \theta dr d\theta d\Phi \\ = \pi \epsilon_2'' \left| E_0 \frac{\epsilon_1 - \epsilon_2}{(\epsilon_1 + 2\epsilon_2)} \right|^2 a^6 \left( \frac{1}{a^3} - \frac{1}{R^3} \right) \quad (16)$$

where  $\epsilon_2''$  is the imaginary part of the dielectric function of silicon. Taylor expansion of Eq. (8) yields

$$W_{\text{abs, Si}}(R) = \frac{4\pi \text{Re}(k_2) k_2'' |E_0|^2 R^3}{3\mu_0 \omega} + O((k_2'' R)^3) \quad (17)$$

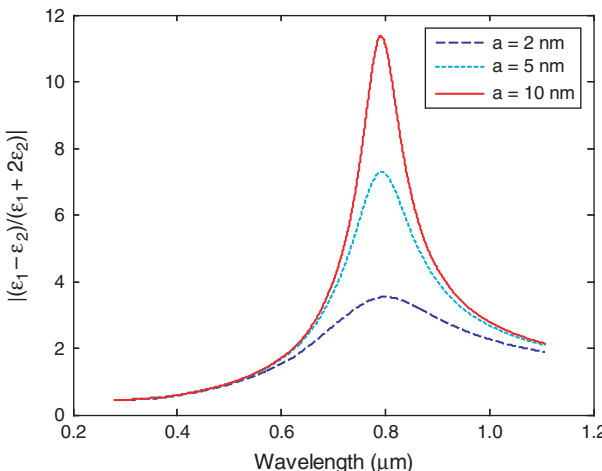


**Fig. 4.** The magnitude of  $|(\epsilon_1 - \epsilon_2)/(\epsilon_1 + 2\epsilon_2)|$ . The peaks for all three particles are centered at around  $0.8 \mu\text{m}$ .

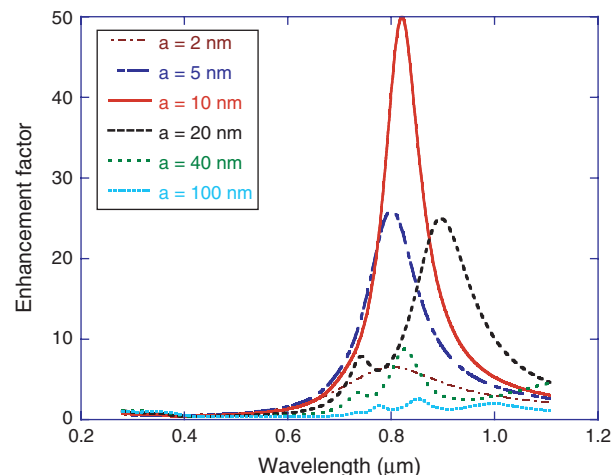


**Fig. 5.** The wavelength dependent enhancement factors for particles with different radii. For all cases,  $R$  is chosen to be  $1.26a$ . The enhancement factor induced by a  $10 \text{ nm}$  particle is 50 at the resonance wavelength.

The absorption enhancement ratio is then given by

$$\gamma(R, a) = \frac{3\mu_0 \omega \epsilon_2'' |(\epsilon_1 - \epsilon_2)/(\epsilon_1 + 2\epsilon_2)|^2}{4\text{Re}(k_2) k_2'' R^3} \\ \times \left[ \left( \frac{a}{R} \right)^3 - \left( \frac{a}{R} \right)^6 \right] \quad (18)$$

which reaches maximum when  $R/a = \sqrt[3]{2}$ , i.e.,  $R = 1.26a$ , as confirmed in Figure 2 for the  $5 \text{ nm}$  and  $10 \text{ nm}$  cases. As for the larger particles, retardation effects push the maximums to smaller  $R$  values.

We have studied the field enhancement at a fixed wavelength heretofore. Figure 5 shows the wavelength dependent absorption enhancement with  $R = 1.26a$ . As seen from the figure, the absorption is enhanced up to 50 times with the presence of the  $10 \text{ nm}$  silver particle. Decrease of the radius from  $10 \text{ nm}$  to  $5 \text{ nm}$  and  $2 \text{ nm}$  leads to dramatic reduction in absorption. A similar trend is seen when increasing the radius of the particles, where the larger  $20 \text{ nm}$ ,  $40 \text{ nm}$  and  $100 \text{ nm}$  particles give less absorption. Nevertheless, the enhancement for all particles is most significant in the wavelength regime between  $0.7 \mu\text{m}$  and  $1.1 \mu\text{m}$ , where the silicon does not absorb light adequately. As shown in the figure, the smaller  $2 \text{ nm}$ ,  $5 \text{ nm}$  and  $10 \text{ nm}$  particles have the maximum absorption at around  $0.8 \mu\text{m}$  with slight shifting of the peaks, while the larger  $20 \text{ nm}$ ,  $40 \text{ nm}$  and  $100 \text{ nm}$  particles have multiple absorption peaks shifted to longer wavelengths. For the small particles, the slight shifting of the absorption peaks from the plasmon wavelength comes from the combined effects of weak retardation and additional wavelength dependent  $\epsilon_2''/\text{Re}(k_2) k_2''$  term in Eq. (18); for the larger particles, the shifting of the absorption peak is due to the retardation effect, which causes a more pronounced variation from the resonance wavelength of  $0.8 \mu\text{m}$ . The results suggest that a

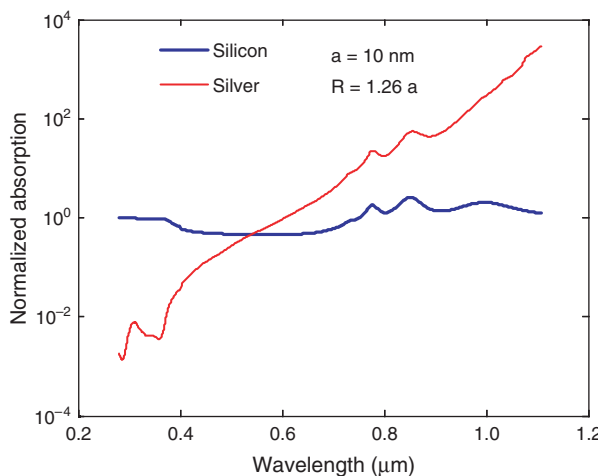


**Fig. 6.** The absorption in a 10 nm silver particle. The absorption loss is significant in the long-wavelength regime.

wide spectrum range can be covered by carefully selecting and mixing particles with different radii.

As revealed in our analysis, the absorption enhancement is caused by the field magnification due to the surface plasmons. However, the surface waves extend to both sides of the interface. Therefore, the unwanted absorption inside the silver particles is inevitably increased along with the absorption enhancement in silicon. Figure 6 shows the wasted absorption in a 10 nm particle and the absorption in the outside shell ( $R = 1.26a$ ). The absorption is normalized to  $W_{\text{abs}, \text{Si}}$  ( $1.26a$ ). For wavelengths larger than  $0.5 \mu\text{m}$ , the silver particle absorbs significantly more light than silicon, especially in the long wavelength range, which presents a problem for the overall optical absorption efficiency. One possible solution is to use the core-shell structure<sup>21</sup> which has a very thin layer of metal that the corresponding absorption loss may be alleviated.

#### 4. SUMMARY

In summary, we have studied the surface-plasmon enhanced absorption in silicon medium. Both extended Mie theory and dipole approximation have been used for the calculations. The field concentration effects of the surface plasmon are examined. The enhancement is found to be mostly confined in a spherical shell surrounding the particle and the optimal thickness of the shell is  $0.26a$ . The spectral analysis shows that the long-wavelength optical absorption in silicon can be enhanced significantly by embedded silver nanoparticles. Enhancement up to 50 times is obtained with a 10 nm silver particle while

smaller and larger particles yield less enhancement. The calculation reveals that the energy loss inside the silver particles may present a problem for efficient energy utilization, which could be potentially addressed by using novel nanostructures. We want to point out that our calculation is based on local field enhancement induced by a single particle. Particle-particle interaction can potentially lead to even higher enhancement. Anisotropic scattering from particles may also give additional enhancement by randomizing the incident solar light.

**Acknowledgments:** We would like to thank Mr. Vincent Berube for helpful comments. This work is partially supported by DOE (Grant No. DE-FG02-02ER45977) and MASDAR.

#### References

1. M. A. Green, *Prog. Photovolt: Res. Appl.* 7, 317 (1999).
2. J. Zhao, A. Wang, P. Altermatt, and M. A. Green, *Appl. Phys. Lett.* 66, 3636 (1995).
3. Air Mass 1.5 Spectra, American Society for Testing and Materials, <http://rredc.nrel.gov/solar/spectra/am1.5/>.
4. K. Yamamoto, A. A. Nakajima, M. Yoshimi, T. Sawada, S. Fukuda, T. Suezaki, M. Ichikawa, Y. Koi, M. Goto, T. Meguro, T. Matsuda, M. Kondo, T. Sasaki, and Y. Tawada, *Sol. Energy* 77, 939 (2004).
5. D. Derkacs, S. H. Lim, P. Matheu, W. Mar, and E. T. Yu, *Appl. Phys. Lett.* 89, 093103 (2006).
6. S. Pillai, K. R. Catchpole, T. Trupke, and M. A. Green, *J. Appl. Phys.* 101, 093105 (2007).
7. B. P. Rand, P. Peumans, and S. R. Forrest, *J. Appl. Phys.* 96, 7519 (2004).
8. G. Zhao, H. Kozuka, and T. Yoko, *Thin Solid Films* 277, 147 (1996).
9. C. Kittel, *Introduction of Solid State Physics*, Wiley, New York (1996).
10. H. Raether, *Surface Plasmons on Smooth and Rough Surfaces and on Gratings*, Springer-Verlag, Berlin (1988).
11. R. K. Chang and T. E. Furtak (eds.), *Surface Enhanced Raman Scattering*, Plenum, New York (1982).
12. K. R. Catchpole and S. J. Pillai, *J. Appl. Phys.* 100, 044504 (2006).
13. C. F. Bohren and D. R. Huffman, *Absorption and Scattering of Light by Small Particles*, Wiley, New York (1983).
14. I. W. Sudiarta and P. Chylek, *J. Opt. Soc. Am. A* 18, 1275 (2001).
15. W. C. Mundy, J. A. Roux, and A. M. Smith, *J. Opt. Soc. Am.* 64, 1593 (1974).
16. P. B. Johnson and R. W. Christy, *Phys. Rev. B* 6, 4370 (1972).
17. E. D. Palik (ed.), *Handbook of Optical Constants of Solids*, Academic, Orlando (1985).
18. W. T. Doyle, *Phys. Rev.* 111, 1067 (1958).
19. C. G. Granqvist and O. Hunderi, *Phys. Rev. B* 16, 3513 (1977).
20. J. D. Jackson, *Classical Electrodynamics*, Academic, New York (1998).
21. E. Prodan, C. Radloff, N. J. Halas, and P. Nordlander, *Science* 302, 419 (2003).

Received: 2 February 2008. Accepted: 3 March 2008.